Double-sided Hybrid Laser-Arc Welding of 25 mm S690QL High Strength Steel

Sørensen, Christian Buhl; Aakjær Ritz Nissen, Alexander; Brynning, Christian; Nielsen, Jeppe Valentin; Schøn, Rasmus; De waal Malefijt, Robert Mateo; Kristiansen, Morten

Published in:
IOP Conference Series: Materials Science and Engineering

DOI (link to publication from Publisher):
10.1088/1757-899x/1135/1/012004

Publication date:
2021

Document Version
Publisher's PDF, also known as Version of record

Double-sided Hybrid Laser-Arc Welding of 25 mm S690QL High Strength Steel

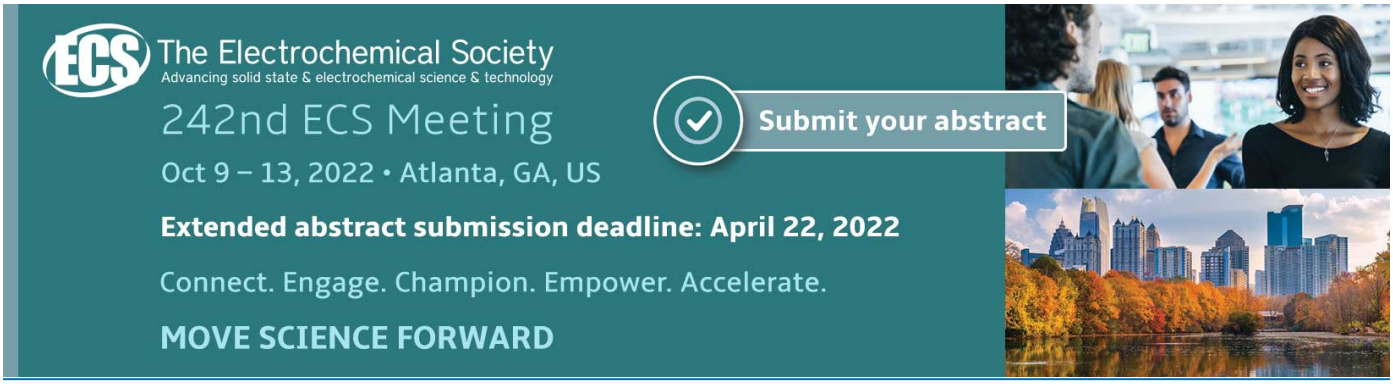

IOP Conf. Series: Materials Science and Engineering 1135 (2021) 012004 doi:10.1088/1757-899X/1135/1/012004

Double-sided Hybrid Laser-Arc Welding of 25 mm S690QL High Strength Steel

C Sørensen[1*], A Nissen[2], C Brynning[2], J Nielsen[2], R Schøn[2], R Malefijt[2] and M Kristiansen[2†]

[1] Siemens Gamesa Renewable Energy, Brande, Denmark
[2] Institute of Materials and Production, Aalborg University, Aalborg, Denmark

[*]christian.soerensen@siemensgamesa.com, [†]morten@mp.aau.dk

Abstract. Hybrid Laser-Arc Welding (HLAW) technique is an enabler for the next generation high efficiency we lding, bu t in dustrial ad option ha s be en li mited du e to pr ocess complexity. Previously documented challenges with root cracks posed by incomplete penetration were significant; h owever, t his w ork p resents s uccessful w eld s amples p repared f rom S 690QL steel welded from two sides with a 16 kW disc laser. Weld travel speeds below 500 mm/min and weld line energies between 1.7 and 1.9 kJ/mm gave sound weld samples, evaluated for yield strength, elongation, hardness and Charpy-V toughness according to DS/EN ISO 10025-6:2004+A1. The results shown here indicate a significant i n t he o verall e fficiency of but t wel ds in high strength steels and further cement the HLAW process for high strength steels. It is shown that the consecutive nature of the weld procedure led to non-negligible interpass temperatures for the second weld.

Keywords: hybrid welding, toughness, interpass temperature, double-sided welding, S690QL, weldability, weld quality

1. Introduction

Demanding applications in fields such as construction and machine building utilize high strength, water-quenched steels to reduce dead mass while maintaining the structure's load-carrying capacity. Multipass welds are necessary for thicknesses beyond 5 mm, and these pose significant risks of excessive heat input, which leads to distortion and deteriorates material properties[1].

Hybrid Laser-Arc Welding (HLAW) combines a high power laser with a conventional Gas Metal Arc Welding (GMAW) torch to achieve deeper penetration, the addition of filler material and higher speed[2] compared to conventional arc welding. The laser beam's high power density results in a narrow and deep heat affected zone without the vacuum requirements necessary for electron-beam welding.

Melt containment is a critical challenge in thick section welding. Previous work on S690QL steel has achieved single pass welding on 15 mm[3] and 20 mm[4, 5]. The melt's surface tension must be sufficient to keep the liquid metal in the weld, and this prerequisite becomes harder to fulfil with increasing plate thickness[6]. Magnetic melt containment has been explored[7], which

could also improve filler wire dilution[8]. Just-in-time induction preheating of welds has also been investigated for S690QL[4, 9, 10], and it was found that the increased thermal input was beneficial for the mechanical properties. A similar sensitivity to thermal input has also been shown in higher grade steels with a yield strength of 960 MPa[11].

Due to the rapid cooling rates generated by the extreme power density of the laser[12, 13], there is a high likelihood for vertical cracks in the root zone of the weld. The cracks have previously been mitigated by increasing the laser energy input and preheating of the base material[14]. Double-sided welds have previously been shown in S355 steel, where the aim was an increase of the penetration capability[15] to 50 mm in steel, and up to 30 mm in aluminium[16]. It has both been shown that the mechanical properties improve from a double-sided weld[17] and that significant issues with hot cracking arise from the partial penetration nature of the weld[18] at high welding speeds.

This work addresses a gap in the previous body of work by investigating double-sided welds in S690QL high strength steel. Strenx 700E is chosen as it is the steel quality with the highest yield strength, that does not require preheating before arc welding. It is relevant to investigate whether this holds for HLAW processes as well. Interpass- or preheating is implemented directly due to the first side HLAW pass, which supports full penetration from a second pass on the other side. The principle can provide a beneficial impact for industrial applications by improving thermal input volumetric control. An experimental approach is applied to identify weld parameters that lead to successful welds, and a numerical model is used to support the hypothesis of interpass heating.

2. Experimental procedure

Weld samples were prepared by water jet cutting of 25 mm SSAB Strenx®700E plate. The steel conforms to DS/EN ISO 10025-6:2004+A1 as S690QL, alloyed according to Table 1, with a resulting carbon equivalent of 0.32 (CEV)/0.49 (CET)[19][1]. The internal weld faces were milled flat and perpendicular before lead-in and -out plates of identical material were welded on to either end of the 130 mm seam, with shims to provide the 0.3 mm gap in the I groove geometry. The samples were subsequently welded using a 1030 nm, 16 kW disc laser (Trumpf TruDisk 16002) and a Fronius TransPuls Synergic 5000 inverter welding power source. The HLAW principle is outlined in figure 1, where relevant setup parameters are annotated.

The GMAW torch and optical elements were mounted on a fixture plate driven by a Fanuc M-710 robot. ESAB OK Aristorod 69 filler wire was used in combination with 82% Ar / 18% CO2 active welding gas. Table 1 outline the fixed experimental parameters and figure 2 shows the top-view geometry of the sample.

Table 1: Chemical composition of SSAB Strenx®700 E [19] and ESAB OK Aristorod 69 [20] given as maximum percentages by mass.

	C	Si	Mn	P	S	Cr	Cu	Ni	Mo	B
Base material	0.20 %	0.60 %	1.60 %	0.020 %	0.010 %	0.8 %	0.30 %	2.0 %	0.70 %	0.005 %
ESAB OK Aristorod 69	0.089 %	0.53 %	1.54 %	-	-	0.26 %	-	1.23 %	0.24 %	-

Twenty-nine samples were welded with varying weld speeds and laser powers, where the bottom side weld was performed first. Secondly, the top side weld was performed after flipping the sample and realigning the robot path to the open groove on the second side. The second

[1] CEV $= C + Mn/6 + (Cu + Ni)/15 + (Cr + Mo + V)/5$ and CET $= C + (Mn + Mo)/10 + (Cr + Cu)/20 + Ni/40$, in mass percentages

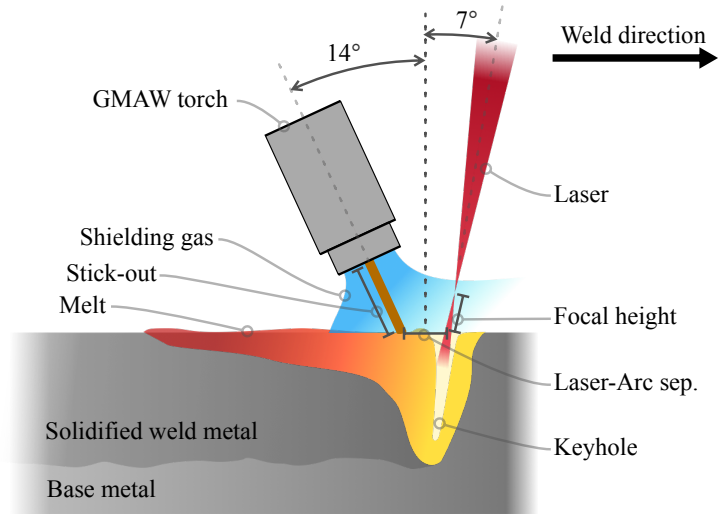

Figure 1: Principle schematic of the HLAW technology, where the primary procedure dimensions are outlined. The weld direction indicates the laser beam movement and arc source relative to a stationary weld sample.

Table 2: Fixed equipment parameters

Focal length of laser optics	600 mm
Focal height	0 mm
Laser angle (w.r.t. vert.)	7°
GMAW torch angle	14°
Wire feed	6 m min^{-1}
Wire diameter	1.6 mm
Stick-out	15 mm
Laser-Arc separation	15 mm
Gas flow	25 L min^{-1}

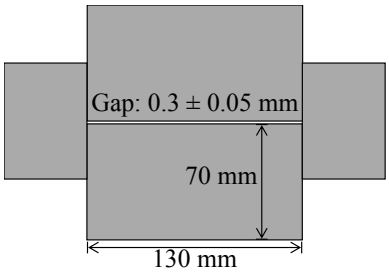

Figure 2: Weld sample geometry. Waterjet cut from 25 mm plate and milled on the internal weld face. The samples are symmetric w.r.t. the root gap. Run-in and run-out plates are shown on the sides.

weld's timing was not controlled but is estimated to be 2 to 3 minutes between the stop of the first weld and the start of the second weld.

The samples were welded with speeds between 300 mm/min and 800 mm/min, in steps of 100 mm/min. The laser power was set between 8 kW and 16 kW, in steps of 2 kW, with the remaining parameters set according to Table 2. Some samples were not finished or analyzed due to melt drooping or insufficient penetration of the weld.

The samples were subjected to tests, according to selection criteria outlined in table 3.

3. Experimental Results

Of the 29 samples, four were discarded due to insufficient penetration, and six were discarded due to drooping.

Nineteen samples were subjected to radiographic inspection, according to DS/EN ISO 10675-1 assessment grade B. As the plate thickness is $\geq$ 25 mm, an Image Quality Indicator (IQI) 10 is used to assess the sensitivity. IQI level 8 is identifiable on the images, corresponding to a sensitivity of 1.6%, fulfilling the requirement of 2% from DS/EN ISO 17636-2.

Table 3: Sample triage definition.

Step	Action	Rule-out criteria
1	Visual inspection of the first weld	Drooping rules the sample out for further processing or inspection.
2	Sectional Imaging	Incomplete penetration rules the sample out from further inspection.
3	Radiographic analysis	Identification of root cracks includes it in the following text but rules out the sample from further analysis.
	Subsequent steps are done in parallel for remaining samples	
4a	Tensile test	
4b	Hardness test	
4c	Charpy V toughness test	

The radiographic inspection discarded 14 samples due to severe pores or root cracks. Macrographs were cut and analyzed in cases of uncertain differentiation between pores and cracks. Five samples were accepted from the radiographic inspection - as indicated in figure 3. Samples were named according to the applied laser power (kW) and travel speed (mm/min): Samples *14/500*, *12/400*, *12/500*, *10/400*, *10/500* was subjected to further analysis.

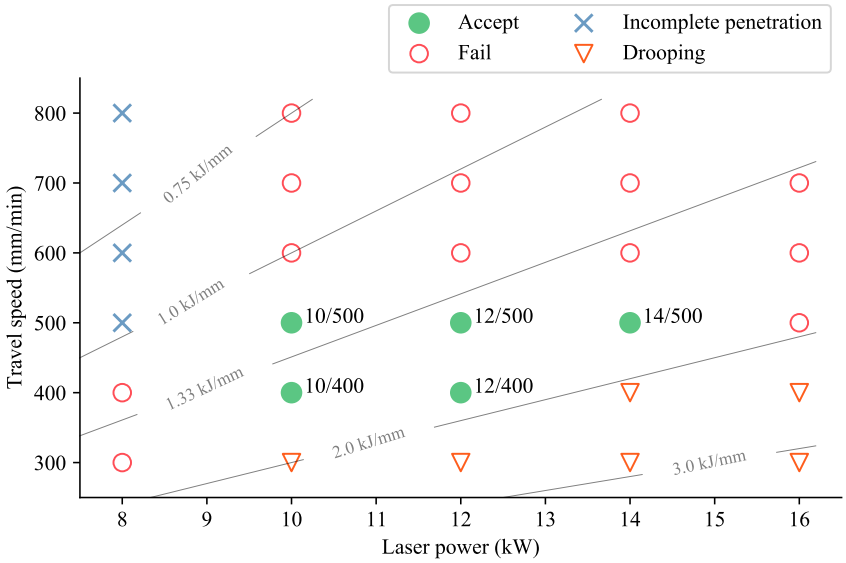

Figure 3: Investigated parameter space. Samples accepted according to DS/EN ISO 10675-1 level B are shown and labeled in green. Samples that failed, had incomplete penetration or drooping are shown in red circles, blue x's or orange triangles respectively. Labeled grey lines in the background indicate the laser line energy deposition.

Samples that were disregarded due to insufficient penetration of the first weld (less than half the plate thickness) were all welded with a laser power of 8 kW, and at speeds higher than 400 mm/min. Samples that were discarded due to drooping, was in the lower right quadrant of figure 3; above 2 kJ/mm linear energy deposition.

Five samples remained, with weld energies shown in table 4. Macrographs were made to show

Table 4: Input line energies of successful weld samples, distributed on arc, laser and in total. Note that the values reported here, are the output energies of the arc source and laser source.

Symbol		*12/400*	*14/500*	*10/400*	*12/500*	*10/500*
Q_{GMAW}	GMAW line energy (kJ/mm)	0.64	0.5	0.63	0.5	0.51
Q_{laser}	Laser line energy (kJ/mm)	1.8	1.68	1.5	1.44	1.2
Q_{tot}	Total line energy (kJ/mm)	2.44	2.18	2.13	1.94	1.71

the heat-affected zone (HAZ); these are displayed in figure 4. Due to the double-sided process, two HAZs are clearly visible. The penetration depth has a positive correlation to the laser line energy.

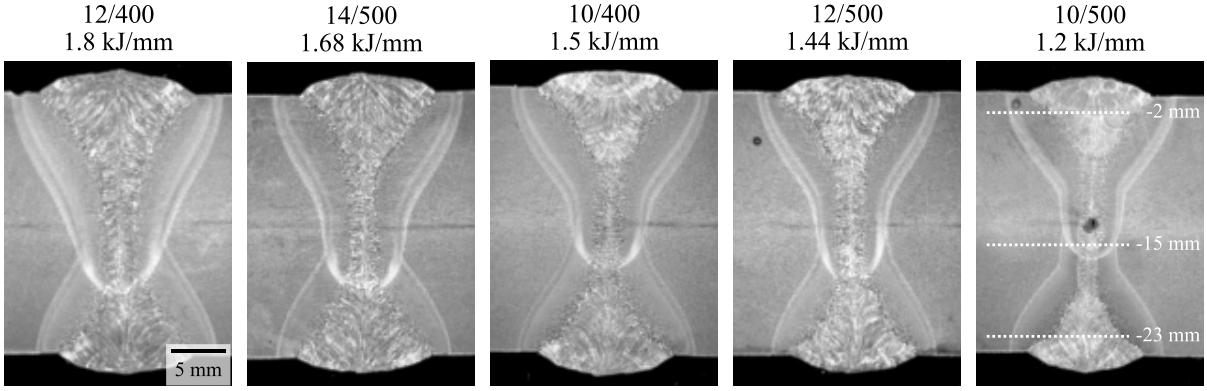

Figure 4: Macrographs of sections of the five remaining samples. The scale bar in *12/400* applies to all macrographs. *10/500* contains annotations to show the position of the hardness measurements presented in figure 5. The dark blemish in the center of *10/500* is a pore, acceptable according to DS/EN ISO 10675-1 level B. Note that the penetration decreases from left to right, in correspondence with the laser line energy from figure 3.

Tensile tests were performed in a Zwick/Roell 100 kN universal testing machine, according to DS/EN ISO 6892-1:2019, to determine the yield strength, ultimate tensile strength and A5 elongation, results shown in table 5. Samples *12/500* and *10/500* is qualified by all tensile test criteria in the base material standard set in DS/EN ISO 10025-6:2004+A1. The tensile test specimens were made to include the root zone from both welds in the center of the 12 mm diameter of the specimen.

Table 5: Results from tensile tests. Results that does not conform to the standard for S690QL are shaded red.

Sample	*12/400*	*14/500*	*10/400*	*12/500*	*10/500*	S690QL
Yield strength (MPa)	608.7	724.7	817.6	846.4	845.5	>690
Ultimate tensile strength (MPa)	756.7	801.2	820.4	847.7	852	770-940
A5 elongation (%)	5.6	5.28	8.1	17	18.18	>14

All macrographic samples are tested for Vickers hardness with a Struers Duramin 40 hardness

tester. Linearly spaced samples are made across the HAZ in three depths, referenced to the surface of the second weld: 2 mm below, 15 mm below (corresponding to the root of the second weld), and 23 mm below to allow comparison to the hardness of the first weld. The positions are noted in figure 4, in pane *10/500*.

The sampled hardness line scans are shown in figure 5, for the five samples. It is observed that the hardness generally increases with decreasing line energy, and that the Vickers hardness near the surface is higher for the first weld than the second weld. Higher line energies provides a more significant preheating, resulting in lower cooling rates and subsequently lower hardness. The first weld is performed on metal with ambient temperature, and experiences greater cooling rates, leading to increased hardness. DS/EN ISO 10025-6:2004+A1 require a hardness below 450HV10, and all weld samples pass this criterion.

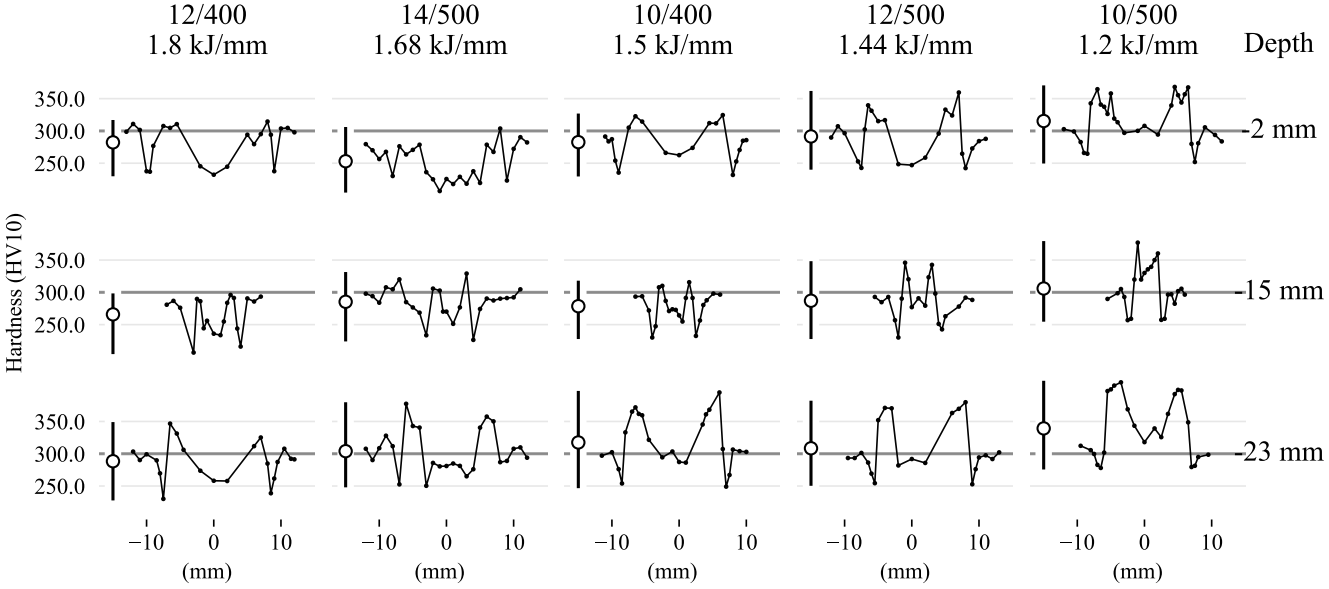

Figure 5: Linearly sampled hardness measurements on the Vickers scale (HV10). The vertical line in each graph spans the maximum and minimum hardness, and the circle show the mean. Note that the peak hardness is higher for samples welded with lower laser line energies (towards the right) and on the first weld surface. Sampled lines are shown in figure 4, pane *10/500.*

Impact toughness at decreased temperatures was tested according to DS/EN ISO 148-1:2006, in a Charpy V-notch apparatus. Samples were prepared with the notch in the HAZ and in the centerline of the weld. While DS/EN ISO 10025-6:2004+A1 specifies a minimum energy absorption of 27 J at −40 °C, SSAB[19] specifies a minimum energy absorption of 69 J for the base material in the transverse direction. Two samples of each configuration (HAZ/weld centre line) were tested.

All samples from the HAZ absorbed more than the instrument's full-scale reading (294 J) and was thus qualifiable. Results from the samples with notches in the weld centerline are shown in figure 6, where the average of the two samples all qualify according to DS/EN ISO 10025-6:2004+A1, but only one weld sample meets the toughness criteria set by SSAB in the base material.

4. Estimation of interpass temperature

A numerical model has been developed to estimate the samples' internal interpass temperature, specifically for the volume relevant to the second weld pass. The manufacturer specifies an

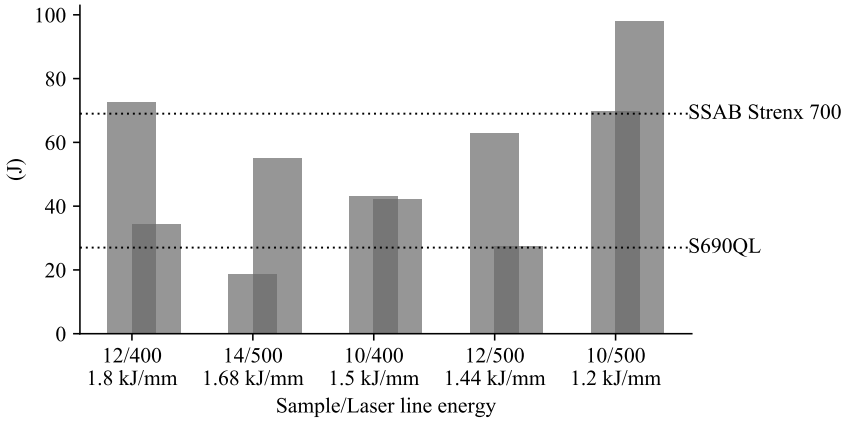

Figure 6: Charpy V-notch impact toughness of the two prepared samples from the weld centerline. All samples except *14/500* meet DS/EN ISO 10025-6:2004+A1, but only *10/500* also meet the base material criteria set by SSAB.

allowable maximum interpass temperature between room temperature and 300 °C[21]

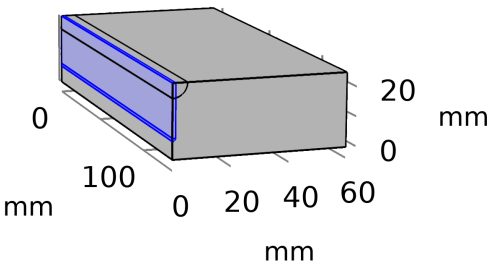

Figure 7: The simulation domains, with the laser deposition volume outlined in blue.

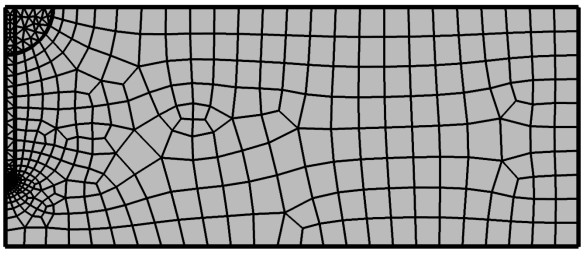

Figure 8: Transverse section of the simulation mesh; it is swept through the longitudinal direction. The third dimension (normal to the paper) is used to implement radiative and convective losses.

The sample volume (excluding the lead in and -out plates) was modelled in the Finite Element software COMSOL Multiphysics 5.4, with geometry as seen in figure 7. Two domains were set up to contain the accumulated energy from the laser source and the GMAW source, each with a thermal efficiency of 80%. At the simulated time $t = 0$, the temperatures in the domains were set according to:

$$T_{\text{arc}}\Big|_{t=0} = T_{\text{amb}} + \frac{E_{\text{arc}}\eta}{C_{\text{p}}\,\rho\,V_{\text{arc}}} \quad \text{and} \quad T_{\text{laser}}\Big|_{t=0} = T_{\text{amb}} + \frac{E_{\text{laser}}\eta}{C_{\text{p}}\,\rho\,V_{\text{laser}}}$$

where T_{arc}, E_{arc}, V_{arc} and T_{laser}, E_{laser}, V_{laser} is the resulting temperature, the accumulated energy (e.g. $E_{arc} = Q_{\text{GMAW}} \cdot 130\,\text{mm}$) and volume of the GMAW and laser domains respectively. T_{amb} is the ambient temperature (20 °C), C_{p} is the thermal capacity of steel ($500\,\text{J}\,\text{kg}^{-1}\,\text{K}^{-1}$), η is the thermal efficiency (80%) and ρ is the density of steel ($7880\,\text{kg}\,\text{m}^{-3}$). For a first order approximation, the temperature dependence of the density and specific heat is not included. Phenomena related to phase transitions in the melt are likewise disregarded. The external boundary conditions model natural convection losses from all exterior sides, as well as

surface-ambient radiative losses. Conductive losses from fixturing are not included, and this overestimates the temperature for longer timescales.

The simulated results are not useful for short timescales due to the large gradients set by the initial boundary conditions. Still, as the sample temperature is renormalized, the simulation converges towards an upper bound of the internal material temperature.

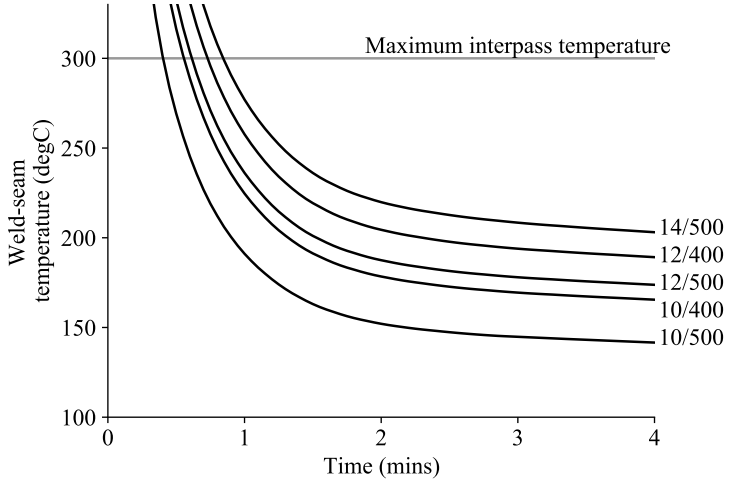

Figure 9: Average temperature of the internal laser weld volume, as a function of time. The five samples are outlined, along with the maximum interpass temperature according to SSAB guidelines [21].

The decay in temperature due to normalization and subsequent losses are shown in figure 9, for boundary conditions corresponding to the five samples' total line energy (laser and arc in their respective domains). It is observed that the temperature after 2 minutes decays less than $20\,^{\circ}\mathrm{C\,min^{-1}}$, only due to convective and radiative losses. At $t = 2$ minutes, the temperatures are between $150\,^{\circ}\mathrm{C}$ to $230\,^{\circ}\mathrm{C}$, and thus well below the SSAB specified allowable interpass temperature of $300\,^{\circ}\mathrm{C}$.

5. Conclusion

Double-sided welding is shown to be successful in joining thick section high strength steel. Samples were tested to fulfil DS/EN ISO 10025-6:2004+A1 and furthermore compared to the higher requirements for the base material from the manufacturer. Two sets of parameters gave weld samples that fulfilled the base material norm, with one parameter set also fulfilling the increased toughness specification from the supplier datasheet.

It was observed in figure 3 that high line energies were necessary to avoid root cracks, that are generally attributed to excessive cooling rates. However, a further increase in line energies resulted in a decrease of material properties like yield strength and elongation (table 5), but also a reduction in peak hardness (figure 5).

The numerical model indicates that the brief duration between the first and second side welds resulted in a non-negligible increase in interpass temperature. The estimated interpass temperature was below the manufacturer's specifications. It is observed that the peak hardness near the surface of the first weld (base material at room temperature) is significantly higher than that of the second weld, performed at elevated temperatures. This work predicts beneficial effects from introducing interpass heating with a double-sided welding process, thus not relying on external equipment such as inductive or flame heating. The remaining heat input that would

otherwise be perceived as waste heat acts to improve the total weld quality. This method could be attractive for industries with a strong focus on environmental optimization.

Acknowledgments
The authors extend their gratitude for funding from Innovation Fund Denmark, project 9066-00007B, "Hybrid Laser-Arc Welding for Offshore Turbine Structures". The authors declare no conflicts of interest. The numerical model is available upon request.

ORCID iDs

C Sørensen	https://orcid.org/0000-0002-3473-0904
A Nissen	https://orcid.org/0000-0002-7602-9008
C Brynning	https://orcid.org/0000-0002-5547-3038
J Nielsen	https://orcid.org/0000-0001-5274-2979
R Schøn	https://orcid.org/0000-0001-5964-7333
R Malefijts	https://orcid.org/0000-0003-1552-7633
M Kristiansen	https://orcid.org/0000-0001-9652-3348

References

[1] Webster S, Kristensen J K and Petring D 2008 *Ironmaking & Steelmaking* **35** 496–504
[2] Silva R G N, de Paço C M M, Rodrigues M B, de Sousa J M S, Pereira M, Ramos B B, Schwedersky M B and Gonçalves e Silva R H 2020 *The International Journal of Advanced Manufacturing Technology* **110** 2801–2814
[3] Bakir N, Üstündağ Ö, Gumenyuk A and Rethmeier M 2020 *Welding in the World* **64** 501–511
[4] Lahdo R, Seffer O, Springer A, Kaierle S and Overmeyer L 2014 *Physics Procedia* **56** 637–645
[5] Lahdo R, Seffer O, Springer A, Kaierle S, Collmann M and Schaumann P 2015 *Stahlbau* **84** 1016–1022
[6] Üstündağ Ö, Gook S, Gumenyuk A and Rethmeier M 2019 *Procedia Manufacturing* **36** 112–120
[7] Üstündağ Ö, Avilov V, Gumenyuk A and Rethmeier M 2019 *Metals* **9** 594
[8] Meng X, Bachmann M, Artinov A and Rethmeier M 2019 *Journal of Manufacturing Processes* **45** 408–418
[9] Li L, Mi G, Zhang X, Xiong L, Zhu Z and Wang C 2019 *Optics & Laser Technology* **119** 105606
[10] Li L, Mi G and Wang C 2019 *Journal of Manufacturing Processes* **43** 276–291
[11] Farrokhi F, Siltanen J and Salminen A 2015 *Journal of Manufacturing Science and Engineering* **137** 061012
[12] Gebhardt M O, Gumenyuk A and Rethmeier M 2013 *Advances in Materials Science and Engineering* **2013** 1–8
[13] Farrokhi F, Endelt B and Kristiansen M 2019 *Optics & Laser Technology* **111** 671–686
[14] Bunaziv I, Akselsen O M, Frostevarg J and Kaplan A F H 2019 *The International Journal of Advanced Manufacturing Technology* **102** 2601–2613
[15] Wahba M, Mizutani M and Katayama S 2016 *Materials & Design* **97** 1–6
[16] Jiang Z, Hua X, Huang L, Wu D, Li F and Zhang Y 2018 *The International Journal of Advanced Manufacturing Technology* **97** 903–913
[17] Lei Z, Zhang K, Hu X, Yang Y, Chen Y and Wu Y 2015 *Journal of Materials Engineering and Performance* **24** 4518–4526
[18] Wiklund G, Akselsen O, Sørgjerd A J and Kaplan A F H 2014 *Journal of Laser Applications* **26** 012003
[19] SSAB 2019 Data sheet Strenx® 700 E/F
[20] ESAB 2021 OK Aristorod 69 datasheet
[21] SSAB 2017 SSAB Strenx Welding Brochure